Title
Solar wind conditions leading to efficient radiation belt electron acceleration: A superposed epoch analysis

Journal
Geophysical Research Letters, 42(17)

ISSN
0094-8276

Authors
Li, W
Thorne, RM
Bortnik, J
et al.

Publication Date
2015-09-16

DOI
10.1002/2015gl065342

AGU PUBLICATIONS

Geophysical Research Letters

RESEARCH LETTER
10.1002/2015GL065342

Key Points:
- A superposed epoch analysis is performed for multiple efficient and inefficient acceleration events
- Prolonged southward B_z, high Vx, and low Psw are important for MeV electron acceleration
- Chorus wave intensity is much stronger during efficient acceleration events than inefficient events

Correspondence to:
W. Li,
moonli@atmos.ucla.edu

Citation:
Li, W., R. M. Thorne, J. Bortnik, D. N. Baker, G. D. Reeves, S. G. Kanekal, H. E. Spence, and J. C. Green (2015), Solar wind conditions leading to efficient radiation belt electron acceleration: A superposed epoch analysis, *Geophys. Res. Lett.*, *42*, 6906–6915, doi:10.1002/2015GL065342.

Received 12 JUL 2015
Accepted 11 AUG 2015
Accepted article online 13 AUG 2015
Published online 7 SEP 2015

Solar wind conditions leading to efficient radiation belt electron acceleration: A superposed epoch analysis

W. Li[1], R. M. Thorne[1], J. Bortnik[1], D. N. Baker[2], G. D. Reeves[3], S. G. Kanekal[4], H. E. Spence[5], and J. C. Green[6]

[1]Department of Atmospheric and Oceanic Sciences, UCLA, Los Angeles, California, USA, [2]Laboratory for Atmospheric and Space Research, University of Colorado Boulder, Boulder, Colorado, USA, [3]Space Science and Applications Group, Los Alamos National Laboratory, Los Alamos, New Mexico, USA, [4]NASA Goddard Space Flight Center, Greenbelt, Maryland, USA, [5]Institute for the Study of Earth, Oceans, and Space, University of New Hampshire, Durham, New Hampshire, USA, [6]Space Hazard Applications LLC, Golden, Colorado, USA

Abstract Determining preferential solar wind conditions leading to efficient radiation belt electron acceleration is crucial for predicting radiation belt electron dynamics. Using Van Allen Probes electron observations (>1 MeV) from 2012 to 2015, we identify a number of efficient and inefficient acceleration events separately to perform a superposed epoch analysis of the corresponding solar wind parameters and geomagnetic indices. By directly comparing efficient and inefficient acceleration events, we clearly show that prolonged southward B_z, high solar wind speed, and low dynamic pressure are critical for electron acceleration to >1 MeV energies in the heart of the outer radiation belt. We also evaluate chorus wave evolution using the superposed epoch analysis for the identified efficient and inefficient acceleration events and find that chorus wave intensity is much stronger and lasts longer during efficient electron acceleration events, supporting the scenario that chorus waves play a key role in MeV electron acceleration.

1. Introduction

Outer radiation belt electrons often exhibit highly dynamic variations [*Blake et al.*, 1992; *Li et al.*, 1993; *Friedel et al.*, 2002] due to a competition between various loss and acceleration processes [*Reeves et al.*, 2003; *Li et al.*, 2007; *Fok et al.*, 2008; *Albert et al.*, 2009; *Xiao et al.*, 2009; *Turner et al.*, 2014]. The response of different populations of electrons with various energies to the same geomagnetic storm can be distinctly different, since 10s–100s keV electron fluxes are enhanced rapidly in association with substorm injections while the timescale for the dynamic response of MeV electrons is typically much longer (~day) [e.g., *Li et al.*, 2005; *Meredith et al.*, 2011; *Li et al.*, 2014a; *Turner et al.*, 2014]. In this study, we focus on the analysis of highly relativistic electron dynamics (>1 MeV), since these so-called "killer" electrons are known to pose significant risks to operating satellites and can potentially cause satellite anomalies or failure [*Baker*, 1998; *Webb and Allen*, 2004; *Choi et al.*, 2011].

It is critical to determine the preferential solar wind conditions leading to MeV electron acceleration, since this is a key step toward predicting their evolution based on preceding solar wind conditions. Important solar wind parameters driving relativistic electron dynamics have been extensively studied in the past few decades. *Paulikas and Blake* [1979] and *Baker et al.* [1979] using geosynchronous electron data found that average electron fluxes correlate positively with corresponding averages of the solar wind velocity. A recent "revisited" study by *Reeves et al.* [2011] using a longer-running data set (1989–2010) from the Los Alamos National Laboratory energetic particle instruments has found a triangle-shaped distribution rather than a linear correlation between solar wind speed and electron fluxes, suggesting that the relationship between radiation belt electron fluxes and solar wind velocity is more complex than previously thought. However, in a multievent study using the Wind spacecraft data during solar minimum, *Blake et al.* [1997] found that relativistic electron enhancement depends not only on a substantial solar wind speed increase but also on a southward turning of the interplanetary magnetic field, which is further supported by *Iles et al.* [2002] and *McPherron et al.* [2009]. Southward turning of the interplanetary magnetic field is associated with an increase in the seed electron fluxes from a few tens to a few hundreds of keV, and these seed electron populations can subsequently be accelerated to highly relativistic (>1 MeV) energies [*Baker et al.*, 1998; *Li et al.*, 2012; *Boyd et al.*, 2014; *Jaynes et al.*, 2015]. *Lyatsky and Khazanov* [2008] have examined the relationship between >2 MeV electron fluxes at geosynchronous orbit and solar wind parameters and found that in addition to the positive correlation with the solar wind speed, relativistic electron fluxes decrease with increasing solar wind density. In a very recent paper by *Kim et al*. [2015], they concluded that sustained south oriented or north-south fluctuating interplanetary magnetic field (IMF) B_z and small solar wind density are crucial for electron enhancements at geosynchronous orbit regardless of geomagnetic storms. In summary, previous studies have demonstrated the potential importance of solar wind velocity, interplanetary magnetic field polarity, and solar wind density. However, many of the previous studies [*Paulikas and Blake*, 1979; *Baker et al*., 1986; *Li et al*., 2001, 2005; *Lyatsky and Khazanov*, 2008; *Borovsky and Denton*, 2009; *McPherron et al*., 2009; *Reeves et al*., 2011; *Kim et al*., 2015] have evaluated electron fluxes at geosynchronous orbit, which is well beyond the region where the radiation belt electron fluxes typically peak and also include adiabatic changes which may not represent a net change in electron phase space density (PSD). Therefore, a careful examination is needed to further determine the important solar wind parameters relevant to MeV electron acceleration.

Regarding the dominant acceleration mechanism of radiation belt electrons to MeV energies, a number of studies have clearly shown that chorus waves are fundamentally important for accelerating seed electrons to highly relativistic energies through efficient energy diffusion [*Horne and Thorne*, 1998; *Summers et al*., 2002; *Horne et al*., 2005; *Tao et al*., 2009; *Reeves et al*., 2013; *Thorne et al*., 2013; *Li et al*., 2014a; *Tu et al*., 2014]. On the other hand, radial diffusion caused by ultralow frequency (ULF) waves also plays an important role in redistributing electrons depending on the radial gradient of the electron PSD and thus accounts for either acceleration through inward radial diffusion or loss of energetic electrons to the magnetopause through outward radial diffusion [e.g., *Elkington et al*., 1999; *Hudson et al*., 1999; *Mathie and Mann*, 2000; *Perry et al*., 2005; *Ukhorskiy et al*., 2009; *Huang et al*., 2010; *Turner et al*., 2012]. Therefore, it will be very interesting to compare the chorus and ULF wave evolution during efficient and inefficient electron acceleration events separately to determine their roles in MeV electron acceleration.

In this study, we focus on evaluating important solar wind conditions leading to efficient electron acceleration in the heart of the outer radiation belt using high-resolution electron measurements from Van Allen Probes, which provide excellent coverage over the core region of the Earth's radiation belts. Through a superposed epoch analysis for a number of efficient and inefficient electron acceleration events separately, we clearly identify the essential solar wind conditions leading to MeV electron acceleration. Furthermore, we also perform a superposed epoch analysis of the global chorus wave activity for the selected efficient and inefficient acceleration events to determine their correlation with MeV electron acceleration.

2. Methodology

2.1. Electron Data Analysis From Van Allen Probes

The twin Van Allen Probes [*Mauk et al*., 2012] have provided an excellent platform for measuring wave and particle evolution in the heart of the radiation belts (<6 R_E) since their launch in August 2012. Radiation belt electron evolution is analyzed using the data from the Van Allen Probes Relativistic Electron Proton Telescope (REPT) [*Baker et al*., 2013; *Spence et al*., 2013] instrument, which measures electron fluxes from ~1.8 MeV to >10 MeV with fine resolution in energy (eight different channels) and pitch angle (36 bins) and thus enables us to evaluate the true nonadiabatic changes by calculating electron PSD for constant adiabatic invariants, as discussed below.

2.2. Calculation of Chorus Wave Intensity Using POES Electron Measurements

Chorus wave intensity evolution on a global scale is critical to evaluate the overall contribution of chorus waves to radiation belt electron dynamics. In this study, we adopt a novel technique of calculating chorus wave intensity from the ratio of the precipitated and trapped electron fluxes (30–100 keV) measured by multiple POES satellites to construct the evolution of chorus wave intensity on a global scale. This technique has been validated by analyzing a number of conjunction events [*Li et al*., 2013, 2014b; *de Soria-Santacruz et al*., 2015], and the details of this technique are described in *Li et al*. [2013] and *Ni et al*. [2014]. The great advantage of this technique is that multiple low-altitude POES satellites with a short orbital period (~100 min) enable us to construct a global dynamic model of chorus wave intensity over a broad region of *L* shell and magnetic local time (MLT) for individual events, which cannot be obtained from the limited number of near-equatorially orbiting satellites alone.

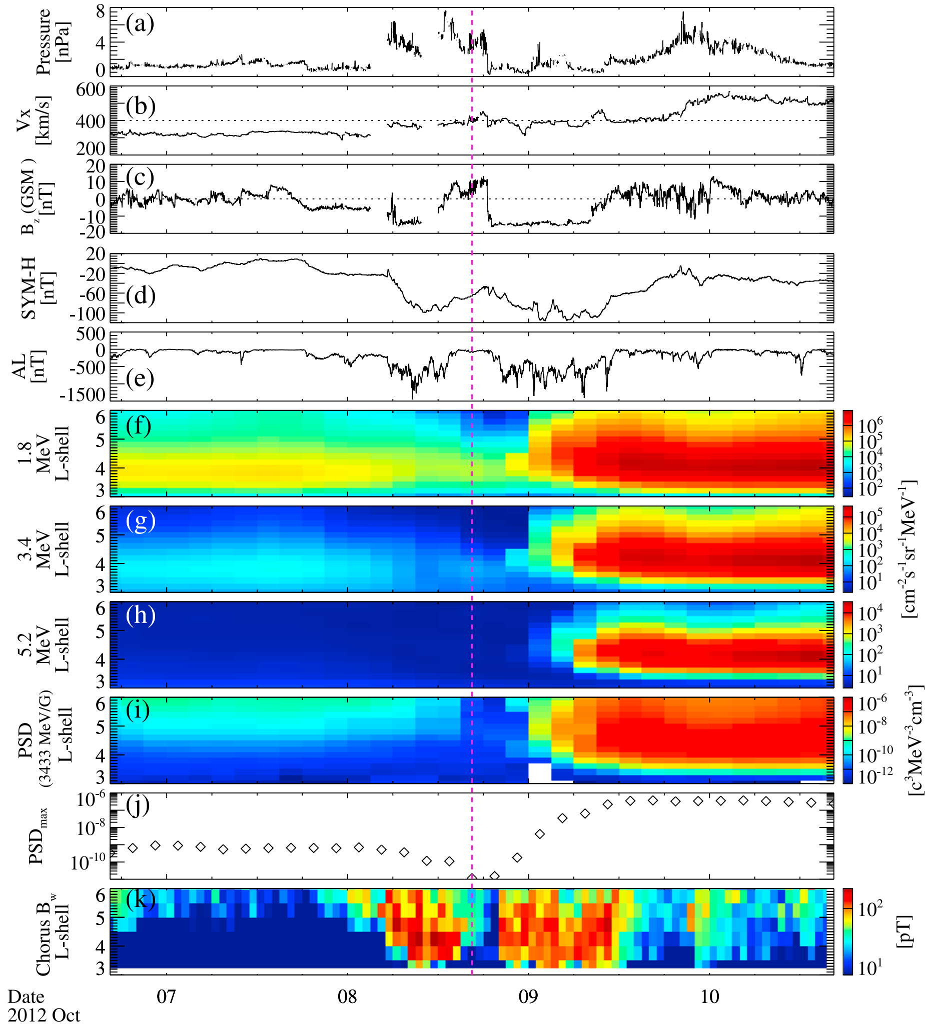

Figure 1. A representative example of an efficient radiation belt electron acceleration event, which occurred during the 8–9 October 2012 storm. (a) Solar wind dynamic pressure, (b) solar wind velocity along the *x* direction, (c) interplanetary magnetic field in *z* direction in GSM coordinate, (d) *SYM-H*, and (e) *AL*. (f–h) Electron fluxes measured by the REPT instrument on Van Allen Probes averaged over each 3 h bin at three different energy channels. (i) Electron phase space density (PSD) calculated for μ = 3433 MeV/G and K = 0.11 $R_E G^{1/2}$, (j) maximum electron PSD over 2.5–6 R_E (PSD_{max}) in each 3 h bin. (k) Chorus wave amplitudes averaged over all MLT sectors as a function of *L* shell. The vertical magenta line represents the zero epoch time used to perform the superposed epoch analysis.

3. Case Analysis for Efficient and Inefficient Acceleration Events

Figure 1 shows an example of an efficient electron acceleration event, which occurred during the 8–9 October 2012 geomagnetic storm, together with solar wind parameters and geomagnetic indices. *SYM-H* index exhibited double dips (Figure 1d) associated with the corresponding disturbances in *AL* (Figure 1e). During the first dip (06–18 UT on 8 October 2012), the solar wind dynamic pressure (Figure 1a) was elevated up to ~8 nPa, the solar wind speed (Figure 1b) remained less than 400 km/s, and the IMF in GSM coordinate (Figure 1c) remained in the southward direction for several hours followed by a northward turning. Electron fluxes (Figures 1f–1h) measured by both Van Allen Probes A and B were averaged every 3 h within each 0.2 *L* bin for various energies (1.8, 3.4, and 5.2 MeV) and exhibited decreases during the first dip. To evaluate the nonadiabatic changes, the electron PSD was calculated for a constant first adiabatic invariant (μ = 3433 MeV/G) and second adiabatic invariant (K = 0.10 $G^{1/2}R_E$) and is shown in Figure 1i as a function of *L* shell. For this given μ = 3433 MeV/G, the corresponding electron energy varies from ~2–3 MeV at ~6 R_E to ~7–8 MeV at ~3 R_E. For the adopted K = 0.10 $G^{1/2}R_E$, the corresponding electron pitch angles change from ~40° to ~90° over the trajectories of Van Allen Probes A and B, which were mostly within 15° of the

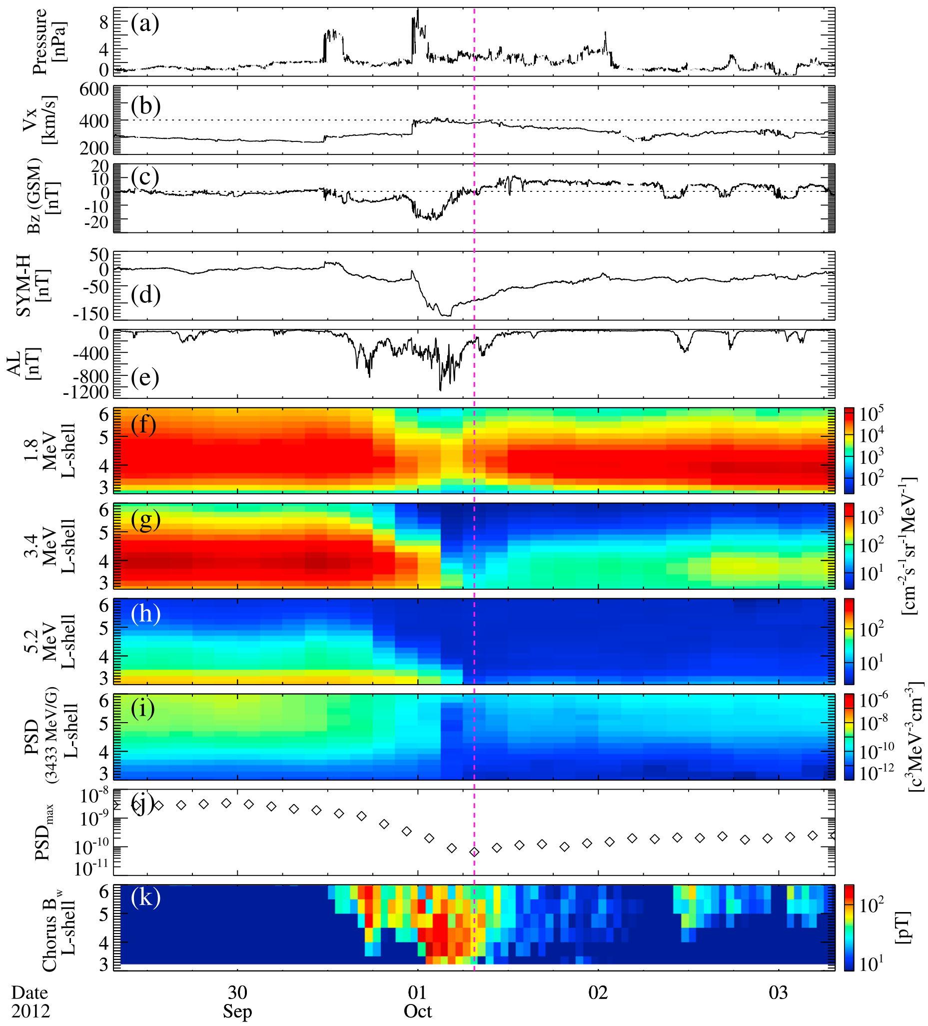

Figure 2. The same format as Figure 1 but for an example of an inefficient acceleration event.

geomagnetic equator. In each 3 h bin, we calculated the maximum PSD (PSD_{max}) over 2.5–6 R_E and show it in Figure 1j. PSD_{max} reached a minimum near the end of the first dip and started to increase substantially during the second dip. We defined the zero epoch time when this PSD_{max} reaches a minimum value, as indicated by the vertical magenta line, and used the same definition in the superposed epoch analysis discussed in section 4. Figure 1k shows chorus wave intensity averaged over all MLT sectors obtained from the POES technique, as mentioned in section 2.2. During the acceleration interval within the second dip, chorus wave intensity was persistently strong for ~16 h over 3–6 R_E, and when chorus wave intensity became weaker after ~12 UT on 9 October 2012, the PSD_{max} was essentially unchanged. These observations support the scenario that chorus waves play a key role in accelerating electrons to the MeV range [*Summers et al.*, 2002; *Horne et al.*, 2005; *Reeves et al.*, 2013; *Thorne et al.*, 2013; *Li et al.*, 2014a; *Tu et al.*, 2014].

Figure 2 shows an inefficient acceleration event, which occurred around 1 October 2012, using the same format as Figure 1. In association with the significant increase in the solar wind dynamic pressure (Figure 2a), multi-MeV electron fluxes (Figures 2f–2h) exhibited a substantial decrease probably due to the dominant magnetopause shadowing effect, as discussed in detail in *Turner et al.* [2014] for this event. During the recovery phase of the storm, the solar wind dynamic pressure remained at a modest value, the solar wind velocity (Figure 2b) was less than 400 km/s, and the IMF was directed in the northward direction for over 24 h, leading to extremely weak substorm activities (Figure 2e). Consequently, MeV electron fluxes barely recovered after the dropout and were much smaller than the prestorm values. Chorus wave activity (Figure 2k) was strong in the prestorm period along with the ongoing substorm activities, but was extremely weak in the recovery

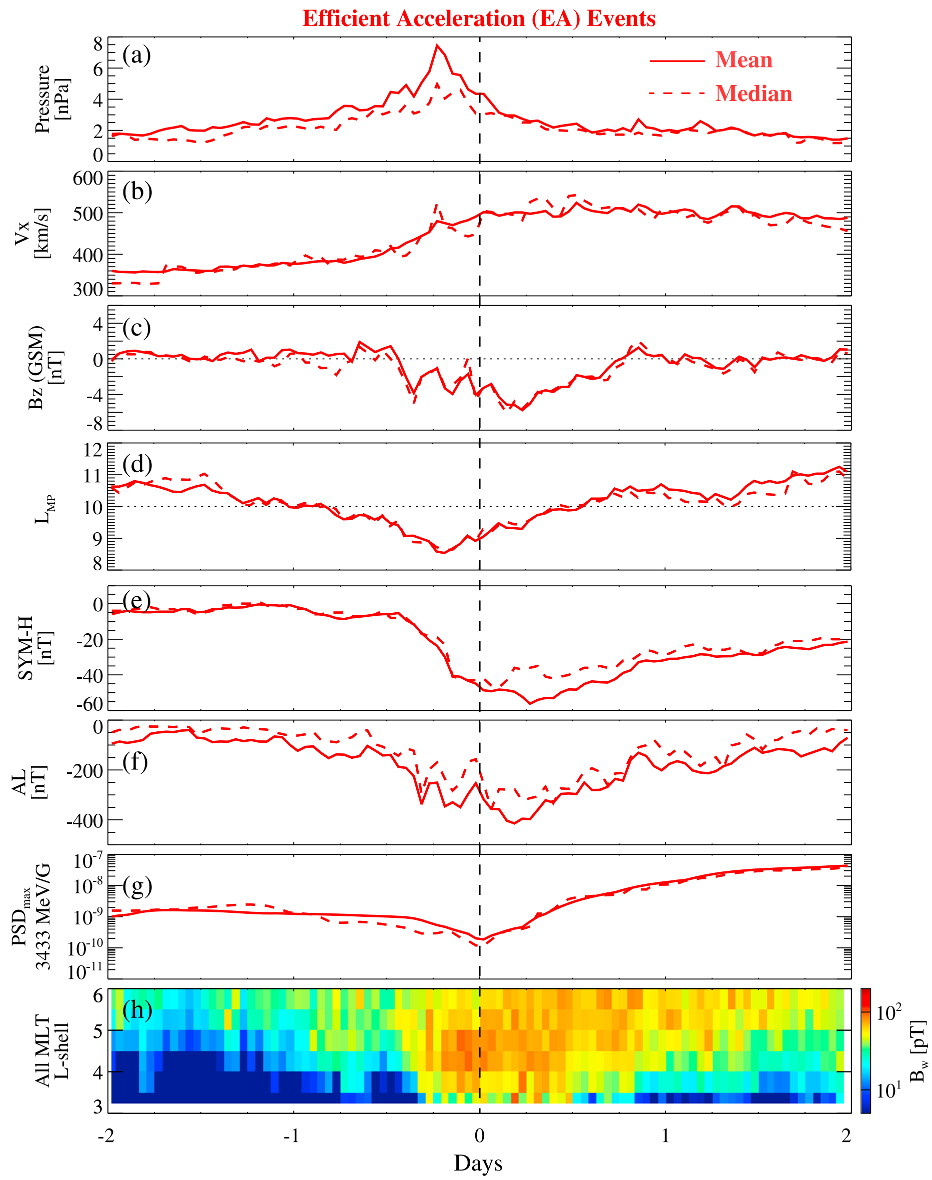

Figure 3. Superposed epoch analysis results of solar wind parameters, magnetopause location (L_{MP}), geomagnetic indices, and electron and chorus wave evolution for 16 efficient acceleration (EA) events. Superposed epoch analysis results of (a) solar wind dynamic pressure, (b) solar wind velocity, (c) B_z, (d) magnetopause location on the subsolar distance, (e) *SYM-H*, (f) *AL*, and (g) PSD_{max}, where the red solid and dashed lines represent the mean and median values, respectively. (h) Superposed epoch analysis result of chorus wave intensity averaged over all MLT sectors using the POES technique as a function of *L* shell. The dashed vertical black line represents the zero epoch time.

phase in association with weak substorm activities. Similarly, we defined the zero epoch time when the PSD_{max} reached a minimum (dashed vertical magenta line) and used it in the following superposed epoch analysis discussed in section 4.

4. Superposed Epoch Analysis for Efficient and Inefficient Acceleration Events

Over the period from 1 October 2012 to 1 April 2015 we identified 16 efficient acceleration (EA) and 17 inefficient acceleration (IA) events to perform a superposed epoch analysis. We defined an EA (IA) event if the PSD_{max} decreased at least by a factor of 5 within 2 days prior to the zero epoch time and the maximum PSD_{max} within 2 days after the zero epoch time is larger (smaller) than 10^{-8} (10^{-9}) $c^3\,MeV^{-3}\,cm^{-3}$. We note that we did not limit the event selection to geomagnetic storms but selected the events based

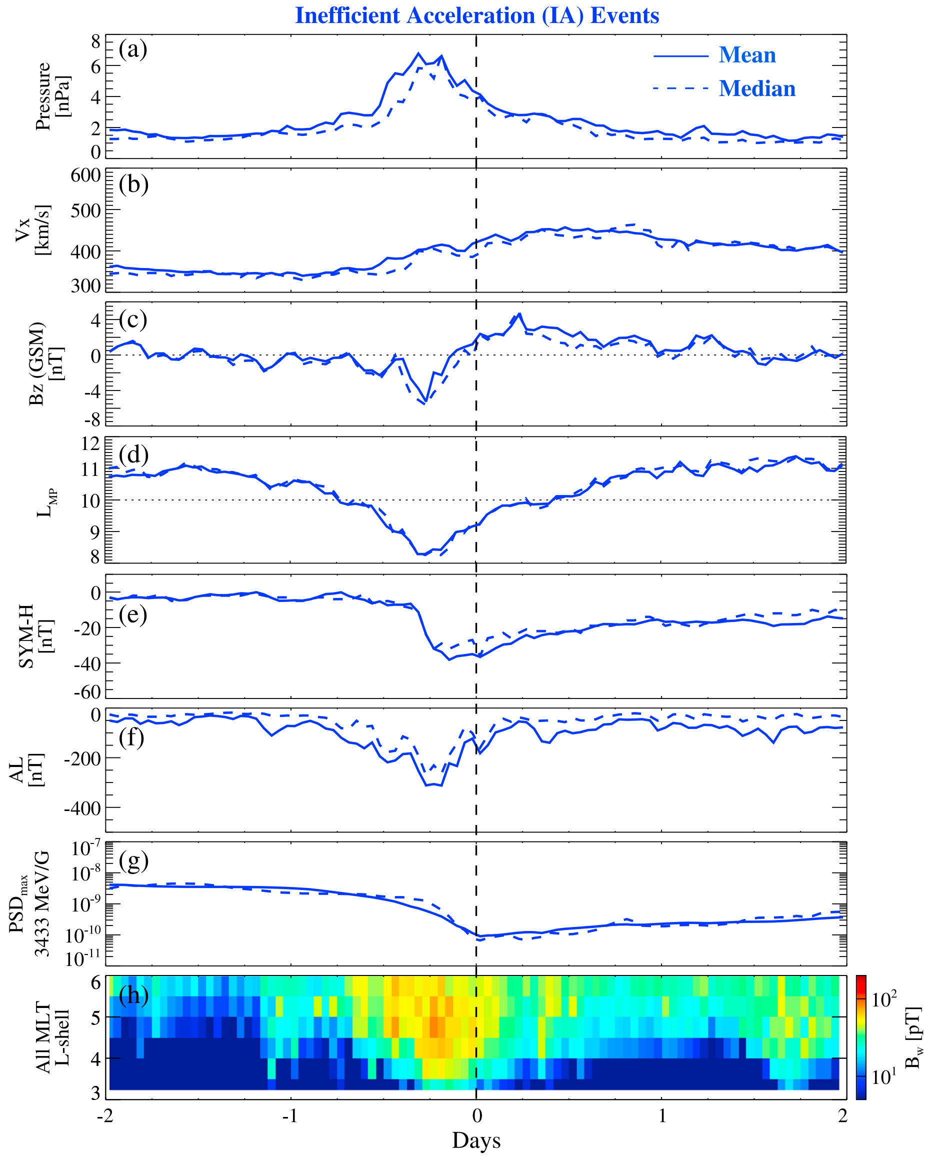

Figure 4. The same format as Figure 3 but for the superposed epoch analysis results of 17 inefficient acceleration (IA) events.

on electron PSD_{max} evolution. This definition allows us to identify the clear EA and IA events regardless of the geomagnetic storm size.

Figure 3 shows the superposed epoch analysis result for 16 EA events. As shown in Figure 3g, electron PSD_{max} starts to rise at around the zero epoch time, after which the solar wind dynamic pressure (Figure 3a) was mostly <2 nPa, the solar wind velocity (Figure 3b) was elevated to ~500 km/s. The most intriguing feature is the prolonged southward IMF B_z (Figure 3c) present after the zero epoch time lasting for longer than 16 h, which is associated with strong disturbances in both *SYM-H* (Figure 3e) and *AL* (Figure 3f) and favorable for providing source and seed electron populations together with chorus wave intensification [e.g., *Miyoshi and Kataoka*, 2008; *Li et al*., 2012]. However, just prior to the zero epoch time when the electron PSD decreases, the solar wind dynamic pressure substantially increased up to ~8 nPa, the solar wind velocity increased from 350 to ~500 km/s, and B_z remained in the southward direction for ~12 h. As shown in Figure 3d, the magnetopause location on the subsolar distance (L_{MP}) estimated based on the equation in *Shue et al*. [1998] moved inward to $L_{MP} \sim 8.5$ prior to the zero epoch time, but moved out beyond $L_{MP} \sim 10$ during the acceleration interval. Both the high solar wind dynamic pressure and southward B_z are favorable for causing electron dropouts [e.g., *Lyatsky and Khazanov*, 2008;

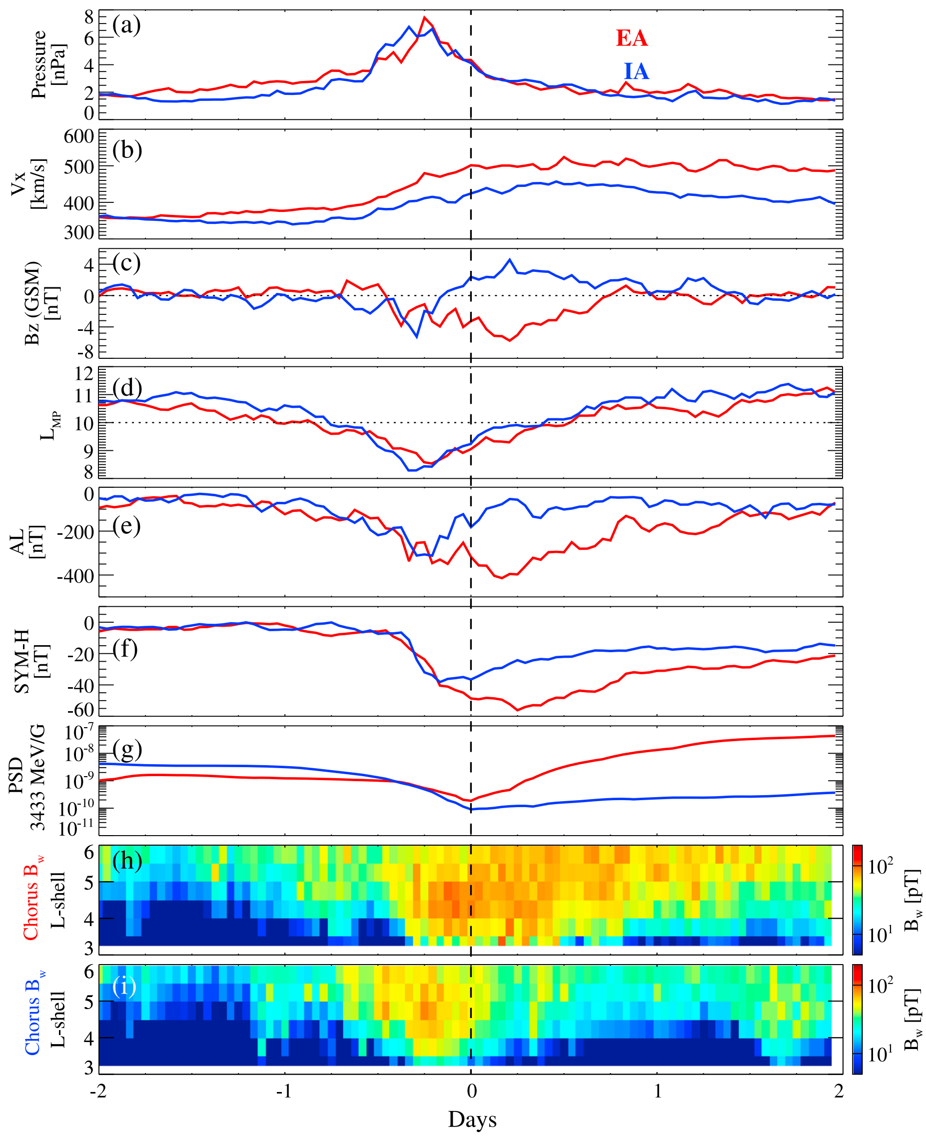

Figure 5. Comparison of the superposed epoch analysis results during EA and IA events. (a–g) The same format as Figures 3a–3g, but overplotted for both EA (red) and IA (blue) events in the same panel. Superposed epoch analysis result of chorus wave intensity using the POES technique during (h) EA and (i) IA events.

Yuan and Zong, 2013; *Gao et al.*, 2015] probably due to the efficient magnetopause shadowing effect followed by the outward radial diffusion process [*Shprits et al.*, 2006; *Turner et al.*, 2012], which is also shown in the inward movement of L_{MP} from ~11 to ~8.5 prior to the zero epoch time. Chorus wave intensity inferred from the POES technique is averaged over a broad range of MLT sectors, and the superposed epoch analysis result for the identified 16 EA events is shown in Figure 3h. The chorus wave intensity is persistently strong within 24 h after the zero epoch time, when the efficient electron acceleration occurs. Moreover, when chorus becomes weaker after 24 h, the electron PSD_{max} also increases much more slowly. These features support the scenario that chorus waves play an important role in accelerating electrons to MeV energies [e.g., *Summers et al.*, 2002; *Horne et al.*, 2005; *Thorne et al.*, 2013]. It is interesting to note that although chorus waves were strong several hours prior to the zero epoch time, the PSD_{max} decreases during this interval probably due to the following reason. Over several hours prior to the zero epoch time, the solar wind dynamic pressure was high and the magnetopause moved closer to the Earth, which favors the magnetopause shadowing loss to be effective and dominant over the chorus-driven electron acceleration, as discussed above.

A superposed epoch analysis is also performed for 17 IA events, and the results are shown in Figure 4. Just after the zero epoch time, the electron PSD_{max} exhibits a very slow recovery (Figure 4g), during which the solar wind dynamic pressure (Figure 4a) was low and the solar wind speed (Figure 4b) was less than 450 km/s. Interestingly, IMF B_z (Figure 4c) remained in the northward direction for over 24 h after the zero epoch time, which led to very weak disturbances in both *SYM-H* (Figure 4e) and *AL* (Figure 4f) together with weak chorus wave intensity (Figure 4h). The magnetopause (Figure 4d) moved inward to $L_{MP} \sim 8$ in association with the PSD_{max} decrease prior to the zero epoch time, but gradually moved out beyond $L_{MP} \sim 10$ subsequently.

In Figures 5a–5g we directly compare the superposed epoch analysis results of the solar wind conditions and geomagnetic indices during EA (red) and IA (blue) events. The most significant difference is that during EA events the IMF B_z (Figure 5c) was persistently in the southward direction during the acceleration interval in contrast to the northward B_z during IA events. The solar wind velocity (Figure 5b) during EA events is larger than that during IA events, whereas the solar wind dynamic pressure (Figure 5a) during EA and IA events after the zero epoch time is comparable. The movement of the magnetopause location (Figure 5d) is not distinctly different during EA and IA events, which may also suggest that the loss driven by the magnetopause shadowing effect is likely to be comparable. The disturbances in *AL* (Figure 5e) and *SYM-H* (Figure 5f) are larger during EA events compared to those during IA events. Moreover, the chorus wave intensity during EA events (Figure 5h) is apparently much stronger and more persistent than that during IA events (Figure 5i), which again supports that chorus waves are fundamentally important for MeV electron acceleration. Therefore, we clearly demonstrate that the most important solar wind conditions leading to efficient electron acceleration include prolonged southward B_z and high solar wind speed. Although not explicitly shown by comparing EA and IA events, the comparison before and after the zero epoch time of EA events clearly suggests that the low solar wind dynamic pressure is also critical to increase the rate of electron acceleration by locating the magnetopause boundary farther away from the Earth, thus minimizing the loss to the magnetopause. For example, in Figure 3 the IMF B_z remains in the southward direction and the solar wind velocity stays high from several hours prior to the zero epoch time, but PSD_{max} only increases after the zero epoch time when the solar wind dynamic pressure becomes low.

5. Summary and Discussion

In the present paper, we determined the preferential solar wind conditions leading to MeV electron acceleration by performing a superposed epoch analysis for a number of efficient and inefficient electron acceleration events separately using the Van Allen Probes electron data from 1 October 2012 to 1 April 2015. Our superposed epoch analysis results clearly show that (1) prolonged southward B_z, (2) high solar wind speed, and (3) low solar wind dynamic pressure are critical to lead to efficient MeV electron acceleration, and the acceleration is most efficient when all three of these conditions are operating simultaneously. We also evaluated the chorus wave evolution using the POES technique [*Li et al.*, 2013; *Ni et al.*, 2014] during efficient and inefficient acceleration events and found that chorus wave intensity is much stronger and lasts longer over a broad region during efficient acceleration events. This is consistent with the scenario that chorus waves play an essential role in MeV radiation belt electron acceleration.

This analysis has been performed using the 2.5 years of Van Allen Probes data from 1 October 2012 to 1 April 2015, which is near the solar maximum of the Cycle 24. Although the data coverage is limited, the Van Allen Probes electron data enable us to evaluate the nonadiabatic changes in MeV electron evolution over a broad region of the outer radiation belt (not limited to the geosynchronous orbit) due to the high-quality electron measurements with fine resolution in both energy and pitch angle. Furthermore, low-altitude electron measurements made by multiple POES satellites provide the global distribution of chorus wave intensity in an event-specific perspective, which cannot be obtained by statistical results or direct wave measurements made by near-equatorially orbiting satellites alone.

Since we have identified the most important solar wind conditions leading to efficient electron acceleration, it will be interesting to use the combination of these parameters to test and further predict the spatiotemporal evolution of the highly relativistic electrons over the entire outer radiation belt. However, this is beyond the scope of the present study and is left for future investigation.

Acknowledgments
This work was supported by JHU/APL contracts 967399 and 921647 under NASA's prime contract NAS5-01072. The analysis at UCLA was supported by the ECT subaward 13–041, NASA grants NNX11AD75G, NNX14AN85G, NNX11AR64G, and NNX13AI61G, and the Air Force Young Investigator program FA9550-15-1-0158. We acknowledge the Van Allen Probes data from the REPT and MagEIS instruments obtained from http://www.rbsp-ect.lanl.gov/data_pub/. We greatly appreciate the NOAA POES data obtained from http://satdat.ngdc.noaa.gov/sem/poes/data/ and the NOAA POES team for providing helpful advice. We also thank the World Data Center for Geomagnetism, Kyoto for providing *SYM-H* and *AL* indices (http://wdc.kugi.kyoto-u.ac.jp/aeasy/index.html), and the Space Physics Data Facility at the NASA Goddard Space Flight Center for providing the OMNI2 data (ftp://spdf.gsfc.nasa.gov/pub/data/omni/omni_cdaweb/).

The Editor thanks George Hoospodarsky and an anonymous reviewer for their assistance in evaluating this paper.

References

Albert, J. M., N. P. Meredith, and R. B. Horne (2009), Three-dimensional diffusion simulation of outer radiation belt electrons during the 9 October 1990 magnetic storm, *J. Geophys. Res.*, *114*, A09214, doi:10.1029/2009JA014336.

Baker, D. N. (1998), What is space weather, *Adv. Space Res.*, *22*, 7–16.

Baker, D. N., P. R. Higbie, R. D. Belian, and E. W. Hones (1979), Do Jovian electrons influence the terrestrial outer radiation zone?, *Geophys. Res. Lett.*, *6*, 531–534, doi:10.1029/GL006i006p00531.

Baker, D. N., J. B. Blake, R. W. Klebesadel, and P. R. Higbie (1986), Highly relativistic electrons in the Earth's outer magnetosphere: 1. Lifetimes and temporal history 1979–1984, *J. Geophys. Res.*, *91*(A4), 4265–4276, doi:10.1029/JA091iA04p04265.

Baker, D. N., et al. (2013), The Relativistic Electron-Proton Telescope (REPT) instrument on board the Radiation Belt Storm Probes (RBSP) spacecraft: Characterization of Earth's radiation belt high-energy particle populations, *Space Sci. Rev.*, *179*, 337–381, doi:10.1007/s11214-012-9950-9.

Baker, D., X. Li, J. Blake, and S. Kanekal (1998), Strong electron acceleration in the Earth's magnetosphere, *Adv. Space Res.*, *21*(4), 609–613, doi:10.1016/S0273-1177(97)00970-8.

Blake, J. B., W. A. Kolasinski, R. W. Fillius, and E. G. Mullen (1992), Injection of electrons and protons with energies of tens of MeV into $L < 3$ on March 24, 1991, *Geophys. Res. Lett.*, *19*, 821–824, doi:10.1029/92GL00624.

Blake, J. B., D. N. Baker, N. Turner, K. W. Ogilvie, and R. P. Lepping (1997), Correlation of changes in the outer-zone relativistic-electron population with upstream solar wind and magnetic field measurements, *Geophys. Res. Lett.*, *24*, 927–930, doi:10.1029/97GL00859.

Borovsky, J. E., and M. H. Denton (2009), Relativistic-electron dropouts and recovery: A superposed epoch study of the magnetosphere and the solar wind, *J. Geophys. Res.*, *114*, A02201, doi:10.1029/2008JA013128.

Boyd, A. J., H. E. Spence, S. G. Claudepierre, J. F. Fennell, J. B. Blake, D. N. Baker, G. D. Reeves, and D. L. Turner (2014), Quantifying the radiation belt seed population in the March 17, 2013 electron acceleration event, *Geophys. Res. Lett.*, *41*, 2275–2281, doi:10.1002/2014GL059626.

Choi, H.-S., J. Lee, K.-S. Cho, Y.-S. Kwak, I.-H. Cho, Y.-D. Park, Y.-H. Kim, D. N. Baker, G. D. Reeves, and D.-K. Lee (2011), Analysis of GEO spacecraft anomalies: Space weather relationships, *Space Weather*, *9*, S06001, doi:10.1029/2010SW000597.

de Soria-Santacruz, M., et al. (2015), Analysis of plasmaspheric hiss wave amplitudes inferred from low-altitude POES electron data: Technique sensitivity analysis, *J. Geophys. Res. Space Physics*, *120*, 3552–3563, doi:10.1002/2014JA020941.

Elkington, S. R., M. K. Hudson, and A. A. Chan (1999), Acceleration of relativistic electrons via drift-resonant interaction with toroidal-mode Pc-5 ULF oscillations, *Geophys. Res. Lett.*, *26*, 3273–3276, doi:10.1029/1999GL003659.

Fok, M.-C., R. B. Horne, N. P. Meredith, and S. A. Glauert (2008), Radiation belt environment model: Application to space weather nowcasting, *J. Geophys. Res.*, *113*, A03S08, doi:10.1029/2007JA012558.

Friedel, R. H. W., G. D. Reeves, and T. Obara (2002), Relativistic electron dynamics in the inner magnetosphere—A review, *J. Atmos. Sol. Terr. Phys.*, *64*, 265–282, doi:10.1016/S1364-6826(01)00088-8.

Gao, X., W. Li, J. Bortnik, R. M. Thorne, Q. Lu, Q. Ma, X. Tao, and S. Wang (2015), The effect of different solar wind parameters upon significant relativistic electron flux dropouts in the magnetosphere, *J. Geophys. Res. Space Physics*, *120*, 4324–4337, doi:10.1002/2015JA021182.

Horne, R. B., and R. M. Thorne (1998), Potential waves for relativistic electron scattering and stochastic acceleration during magnetic storms, *Geophys. Res. Lett.*, *25*(15), 3011–3014, doi:10.1029/98GL01002.

Horne, R. B., et al. (2005), Wave acceleration of electrons in the Van Allen radiation belts, *Nature*, *437*, 227–230, doi:10.1038/nature03939.

Huang, C.-L., H. E. Spence, M. K. Hudson, and S. R. Elkington (2010), Modeling radiation belt radial diffusion in ULF wave fields: 2. Estimating rates of radial diffusion using combined MHD and particle codes, *J. Geophys. Res.*, *115*, A06216, doi:10.1029/2009JA014918.

Hudson, M. K., S. R. Elkington, J. G. Lyon, C. C. Goodrich, and T. J. Rosenberg (1999), Simulation of radiation belt dynamics driven by solar wind variations, in *Sun-Earth Plasma Connections*, edited by J. L. Burch, R. L. Carovillano, and S. K. Antiochos, AGU, Washington, D. C., doi:10.1029/GM109p0171.

Iles, R. H. A., A. N. Fazakerley, A. D. Johnstone, N. P. Meredith, and P. Bühler (2002), The relativistic electron response in the outer radiation belt during magnetic storms, *Ann. Geophys.*, *20*, 957–965, doi:10.5194/angeo-20-957-2002.

Jaynes, A. N., et al. (2015), Source and seed populations for relativistic electrons: Their roles in radiation belt changes, *J. Geophys. Res. Space Physics*, doi:10.1002/2015JA021234, in press.

Kim, H.-J., L. Lyons, V. Pinto, C.-P. Wang, and K.-C. Kim (2015), Revisit of relationship between geosynchronous relativistic electron enhancements and magnetic storms, *Geophys. Res. Lett.*, *42*, doi:10.1002/2015GL065192.

Li, W., Y. Y. Shprits, and R. M. Thorne (2007), Dynamic evolution of energetic outer zone electrons due to wave-particle interactions during storms, *J. Geophys. Res.*, *112*, A10220, doi:10.1029/2007JA012368.

Li, W., R. Thorne, J. Bortnik, R. McPherron, Y. Nishimura, V. Angelopoulos, and I. G. Richardson (2012), Evolution of chorus waves and their source electrons during storms driven by corotating interaction regions, *J. Geophys. Res.*, *117*, A08209, doi:10.1029/2012JA017797.

Li, W., B. Ni, R. M. Thorne, J. Bortnik, J. C. Green, C. A. Kletzing, W. S. Kurth, and G. B. Hospodarsky (2013), Constructing the global distribution of chorus wave intensity using measurements of electrons by the POES satellites and waves by the Van Allen Probes, *Geophys. Res. Lett.*, *40*, 4526–4532, doi:10.1002/grl.50920.

Li, W., et al. (2014a), Radiation belt electron acceleration by chorus waves during the 17 March 2013 storm, *J. Geophys. Res. Space Physics*, *119*, 4681–4693, doi:10.1002/2014JA019945.

Li, W., et al. (2014b), Quantifying hiss-driven energetic electron precipitation: A detailed conjunction event analysis, *Geophys. Res. Lett.*, *41*, 1085–1092, doi:10.1002/2013GL059132.

Li, X., I. Roth, M. Temerin, J. R. Wygant, M. K. Hudson, and J. B. Blake (1993), Simulation of the prompt energization and transport of radiation belt particles during the March 24, 1991 SSC, *Geophys. Res. Lett.*, *20*(22), 2423–2426, doi:10.1029/93GL02701.

Li, X., M. Temerin, D. N. Baker, G. D. Reeves, and D. Larson (2001), Quantitative prediction of radiation belt electrons at geostationary orbit based on solar wind measurements, *Geophys. Res. Lett.*, *28*, 1887–1890, doi:10.1029/2000GL012681.

Li, X., D. N. Baker, M. Temerin, G. Reeves, R. Friedel, and C. Shen (2005), Energetic electrons, 50 keV to 6 MeV, at geosynchronous orbit: Their responses to solar wind variations, *Space Weather*, *3*, S04001, doi:10.1029/2004SW000105.

Lyatsky, W., and G. V. Khazanov (2008), Effect of solar wind density on relativistic electrons at geosynchronous orbit, *Geophys. Res. Lett.*, *35*, L03109, doi:10.1029/2007GL032524.

Mathie, R. A., and I. R. Mann (2000), A correlation between extended intervals of ULF wave power and storm-time geosynchronous relativistic electron flux enhancements, *Geophys. Res. Lett.*, *27*, 3261–3264, doi:10.1029/2000GL003822.

Mauk, B. H., N. J. Fox, S. G. Kanekal, R. L. Kessel, D. G. Sibeck, and A. Ukhorskiy (2012), Science objectives and rationale for the radiation belt storm probes mission, *Space Sci. Rev.*, 1–15, doi:10.1007/s11214-012-9908-y.

McPherron, R. L., D. N. Baker, and N. U. Crooker (2009), Role of the Russell-McPherron effect in the acceleration of relativistic electrons, *J. Atmos. Sol. Terr. Phys.*, *71*, 1032–1044.

Meredith, N. P., R. B. Horne, M. M. Lam, M. H. Denton, J. E. Borovsky, and J. C. Green (2011), Energetic electron precipitation during high-speed solar wind stream driven storms, *J. Geophys. Res.*, *116*, A05223, doi:10.1029/2010JA016293.

Miyoshi, Y., and R. Kataoka (2008), Flux enhancement of the outer radiation belt electrons after the arrival of stream interaction regions, *J. Geophys. Res.*, *113*, A03S09, doi:10.1029/2007JA012506.

Ni, B., W. Li, R. M. Thorne, J. Bortnik, J. C. Green, C. A. Kletzing, W. S. Kurth, G. B. Hospodarsky, and M. de Soria-Santacruz Pich (2014), A novel technique to construct the global distribution of whistler mode chorus wave intensity using low-altitude POES electron data, *J. Geophys. Res. Space Physics*, *119*, 5685–5699, doi:10.1002/2014JA019935.

Paulikas, G. A., and J. B. Blake (1979), Effects of the solar wind on magnetospheric dynamics: Energetic electrons at the synchronous orbit, in *Quantitative Modeling of Magnetospheric Processes*, *Geophys. Monogr. Ser.*, vol. 21, edited by W. P. Olson, pp. 180–202, AGU, Washington, D. C.

Perry, K. L., M. K. Hudson, and S. R. Elkington (2005), Incorporating spectral characteristics of Pc5 waves into three-dimensional radiation belt modeling and the diffusion of relativistic electrons, *J. Geophys. Res.*, *110*, A03215, doi:10.1029/2004JA010760.

Reeves, G. D., K. L. McAdams, R. H. W. Friedel, and T. P. O'Brien (2003), Acceleration and loss of relativistic electrons during geomagnetic storms, *Geophys. Res. Lett.*, *30*(10), 1529, doi:10.1029/2002GL016513.

Reeves, G. D., S. K. Morley, R. H. W. Friedel, M. G. Henderson, T. E. Cayton, G. Cunningham, J. B. Blake, R. A. Christensen, and D. Thomsen (2011), On the relationship between relativistic electron flux and solar wind velocity: Paulikas and Blake revisited, *J. Geophys. Res.*, *116*, A02213, doi:10.1029/2010JA015735.

Reeves, G., et al. (2013), Electron acceleration in the heart of the Van Allen radiation belts, *Science*, doi:10.1126/science.1237743.

Shprits, Y. Y., R. M. Thorne, R. Friedel, G. D. Reeves, J. Fennell, D. N. Baker, and S. G. Kanekal (2006), Outward radial diffusion driven by losses at magnetopause, *J. Geophys. Res.*, *111*, A11214, doi:10.1029/2006JA011657.

Shue, J.-H., et al. (1998), Magnetopause location under extreme solar wind conditions, *J. Geophys. Res.*, *103*(A8), 17,691–17,700, doi:10.1029/98JA01103.

Spence, H. E., et al. (2013), Science goals and overview of the Energetic particle, Composition, and Thermal plasma (ECT) suite on NASA's Radiation Belt Storm Probes (RBSP) mission, *Space Sci. Rev.*, *179*, 311–336, doi:10.1007/s11214-013-0007-5.

Summers, D., C. Ma, N. P. Meredith, R. B. Horne, R. M. Thorne, D. Heynderickx, and R. R. Anderson (2002), Model of the energization of outer-zone electrons by whistler-mode chorus during the October 9, 1990 geomagnetic storm, *Geophys. Res. Lett.*, *29*(24), 2174, doi:10.1029/2002GL016039.

Tao, X., J. M. Albert, and A. A. Chan (2009), Numerical modeling of multidimensional diffusion in the radiation belts using layer methods, *J. Geophys. Res.*, *114*, A02215, doi:10.1029/2008JA013826.

Thorne, R. M., et al. (2013), Rapid local acceleration of relativistic radiation belt electrons by magnetospheric chorus, *Nature*, *504*, 411–414, doi:10.1038/nature12889.

Tu, W., G. S. Cunningham, Y. Chen, S. K. Morley, G. D. Reeves, J. B. Blake, D. N. Baker, and H. Spence (2014), Event-specific chorus wave and electron seed population models in DREAM3D using the Van Allen Probes, *Geophys. Res. Lett.*, *41*, 1359–1366, doi:10.1002/2013GL058819.

Turner, D. L., Y. Shprits, M. Hartinger, and V. Angelopoulos (2012), Explaining sudden losses of outer radiation belt electrons during geomagnetic storms, *Nat. Phys.*, *8*, 208–212, doi:10.1038/Nphys2185.

Turner, D. L., et al. (2014), On the cause and extent of outer radiation belt losses during the 30 September 2012 dropout event, *J. Geophys. Res. Space Physics*, *119*, 1530–1540, doi:10.1002/2013JA019446.

Ukhorskiy, A. Y., M. I. Sitnov, K. Takahashi, and B. J. Anderson (2009), Radial transport of radiation belt electrons due to stormtime Pc5 waves, *Ann. Geophys.*, *27*, 2173–2181.

Webb, F., and J. H. Allen (2004), Spacecraft and ground anomalies related to the October–November 2003 solar activity, *Space Weather*, *2*, S03008, doi:10.1029/2004SW000075.

Xiao, F., Z. Su, H. Zheng, and S. Wang (2009), Modeling of outer radiation belt electrons by multidimensional diffusion process, *J. Geophys. Res.*, *114*, A03201, doi:10.1029/2008JA013580.

Yuan, C. J., and Q. G. Zong (2013), Relativistic electron fluxes dropout in the outer radiation belt under different solar wind conditions, *J. Geophys. Res. Space Physics*, *118*, 7545–7556, doi:10.1002/2013JA019066.